

Auxiliary-field quantum Monte Carlo study of TiO and MnO molecules

W. A. Al-Saidi, Henry Krakauer, and Shiwei Zhang

Department of Physics, College of William and Mary, Williamsburg, VA 23187-8795

(Dated: July 3, 2018)

Calculations of the binding energy of the transition metal oxide molecules TiO and MnO are presented, using a recently developed phaseless auxiliary field quantum Monte Carlo approach. This method maps the interacting many-body problem onto a linear combination of non-interacting problems by a complex Hubbard-Stratonovich transformation, and controls the phase/sign problem with a phaseless approximation relying on a trial wave function. It employs random walks in Slater determinant space to project the ground state of the system, and allows use of much of the same machinery as in standard density functional theory calculations, such as planewave basis and non-local pseudopotentials. The calculations used a single Slater determinant trial wave function obtained from a density functional calculation, with no further optimization. The calculated binding energies are in good agreement with experiment and with recent diffusion Monte Carlo results. Together with previous results for *sp*-bonded systems, the present study indicates that the phaseless auxiliary field method is a robust and promising approach for the study of correlation effects in real materials.

PACS numbers: 02.70.Ss, 71.15.-m, 31.25.-v

I. INTRODUCTION

A phaseless auxiliary field (AF) quantum Monte Carlo (QMC) method was recently introduced [1] to study correlation effects in real materials, which has yielded results for a variety of *sp*-bonded materials in good agreement with experiment and comparable to those obtained using the standard diffusion Monte Carlo method (DMC) [2]. In this paper we present the first application of the phaseless AF QMC method to the more highly-correlated transition metal oxide systems. Because of their complexity (the presence of both localized and itinerant characters in the electronic degrees of freedom, strong electron-ion pseudopotentials, and the presence of many highly correlated electrons), there have been relatively few QMC calculations of any type for transition metal systems [3–6].

There are many important applications based on the magnetic, ferroelectric, and superconducting properties of transition metal oxides. These effects arise from the presence of *d*-shell electrons whose interactions are often highly correlated. The generally successful *ab initio* density functional theory (DFT) approach [7] has had limited success in describing these properties, often predicting incorrect ground states (*e.g.* metallic instead of insulating). Even in cases where correlation effects are less pronounced and the method is qualitatively correct, the results are sometimes not of sufficient accuracy. For example in ferroelectrics such as PbTiO₃, which have essentially no occupied *d*-states, the relatively small and usually acceptable DFT errors (~3%) in predicted equilibrium volumes can lead to suppression of the ferroelectric ground state. There is thus a great need for better theoretical modeling of transition metal systems.

Ab initio quantum Monte Carlo methods are an attractive means to treat *explicitly* the interacting many fermion system. These methods in principle scale algebraically as a low power with system size. However, except for a few special cases, QMC methods are plagued by the fermion sign problem [8, 9], which, if uncontrolled, results in exponential scaling. No formal solution has been found for this problem, but approximate methods have been developed that control it. The most established QMC method is the real space fixed-node diffusion Monte Carlo [10], which has been applied to calculate many properties of solids and molecules [2]. Recent DMC studies have addressed transition metal systems such as the TiC molecule [3], TiO and MnO molecules [4], solid MnO [5], and solid NiO [6].

The new phaseless AF QMC approach [1] is an alternative that has several appealing features. For example, it is formulated in a Hilbert space spanned by some fixed one-particle basis, and the freedom to choose *any* one-particle basis suitable for a given problem could be advantageous. Moreover, the AF QMC methodology can take full advantage of well-established techniques used by independent-particle methods with the same basis. With a planewave basis, for example, algorithms based on fast Fourier transforms (FFT) and separable non-local pseudopotentials can be carried over from DFT planewave codes. Given the remarkable development and success of the latter [11], it is clearly desirable to have a QMC method that can use exactly the same machinery and systematically include correlation effects by simply building stochastic ensembles of the independent-particle solutions.

The central idea in standard AF QMC methods [12, 13] is the mapping of the interacting many-body problem

into a linear combination of non-interacting problems in external auxiliary fields. Averaging over different AF configurations is then performed by Monte Carlo (MC) techniques. However, except for special cases (e.g., the Hubbard model with on-site interactions), the two-body interactions will require auxiliary fields that are *complex*. As a result, the single-particle orbitals become complex, and the MC averaging over AF configurations becomes an integration over complex variables in many dimensions, and a phase problem occurs.

The phaseless AF QMC method [1] used in this paper controls the phase/sign problem in an approximate manner using a trial wave function. As in fixed-node DMC, the calculated results approach the exact ones as the trial wave function is improved. The ground-state energy in the phaseless method, however, is not a variational upper bound [1, 14]. Previous results on *sp*-bonded systems [1, 15] and our current results suggest that the calculated energy is quite insensitive to the trial wave function. Accurate ground-state energies have been obtained with simple trial wave functions, namely single Slater determinants from DFT or Hartree-Fock calculations.

In this paper, we study the transition metal oxide molecules TiO and MnO, using the phaseless AF QMC method with planewaves and pseudopotentials. This represents the first application of AF-based QMC to transition metal oxides. As in regular DFT calculations, molecules can be studied with planewaves by placing them in large cells (supercells) and using periodic boundary conditions. This is somewhat disadvantageous because one has to insure that the supercells are large enough to eliminate the spurious interactions between the images of the molecule. Consequently the computational cost for isolated atoms and molecules is higher than with a localized basis. However, the main motivation of the present study is to test the phaseless AF QMC method for strongly correlated systems such as transition metal oxides, using the same methodology as previously used for *sp*-bonded materials. In addition, a converged planewave basis, which is straightforward to achieve aside from the computational cost, gives an unbiased representation of the Hamiltonian, and facilitates direct comparison with experiment.

The remainder of the paper is organized as follows. The phaseless AF QMC method is briefly reviewed in Sec. II. The specific formulation using a single-particle planewave basis with non-local pseudopotentials is then discussed in Sec. III. Finally, in Sec. IV we present results of our calculations for the binding energies of TiO and MnO, which are in excellent agreement with experiment.

II. FORMALISM

The Hamiltonian for a many-fermion system with two-body interactions can be written in any one-particle basis in the general form

$$\hat{H} = \hat{H}_1 + \hat{H}_2 = \sum_{i,j}^M T_{ij} c_i^\dagger c_j + \frac{1}{2} \sum_{i,j,k,l}^M V_{ijkl} c_i^\dagger c_j^\dagger c_k c_l, \quad (1)$$

where M is the size of the chosen one-particle basis, and c_i^\dagger and c_i are the corresponding creation and annihilation operators. Both the one-body (T_{ij}) and two-body matrix elements (V_{ijkl}) are known.

As in other QMC methods, the auxiliary field quantum Monte Carlo obtains the ground state $|\Psi_G\rangle$ of \hat{H} by projecting from a trial wave function $|\Psi_T\rangle$, using the imaginary-time propagator $e^{-\tau\hat{H}}$:

$$|\Psi_G\rangle \propto \lim_{n \rightarrow \infty} (e^{-\tau\hat{H}})^n |\Psi_T\rangle. \quad (2)$$

The trial wave function $|\Psi_T\rangle$, which should have a non-zero overlap with the exact ground state, is assumed to be in the form of a single Slater determinant or a linear combination of Slater determinants.

Using a second-order Trotter breakup, we write the propagator as:

$$e^{-\tau\hat{H}} = e^{-\tau\hat{H}_1/2} e^{-\tau\hat{H}_2} e^{-\tau\hat{H}_1/2} + \mathcal{O}(\tau^3). \quad (3)$$

The two-body part of the propagator can be written as an integral of one-body operators by a Hubbard-Stratonovich transformation [16]:

$$e^{-\tau\hat{H}_2} = \prod_{\alpha} \left(\frac{1}{\sqrt{2\pi}} \int_{-\infty}^{\infty} e^{-\frac{1}{2}\sigma_{\alpha}^2} e^{\sqrt{\tau}\sigma_{\alpha}\sqrt{\lambda_{\alpha}}\hat{v}_{\alpha}} d\sigma_{\alpha} \right), \quad (4)$$

after \hat{H}_2 is turned into a sum of squares of one-body operators: $\hat{H}_2 = -\frac{1}{2} \sum_{\alpha} \lambda_{\alpha} \hat{v}_{\alpha}^2$, with λ_{α} a real number.

The propagator of Eq. (3) can now be expressed in the general form:

$$e^{-\tau\hat{H}} = \int P(\sigma) \mathcal{B}(\sigma) d\sigma, \quad (5)$$

where we have introduced the vector representations $\sigma \equiv \{\sigma_1, \sigma_2, \dots\}$, $P(\sigma)$ is the normal distribution with mean 0 and standard deviation 1, and

$$\mathcal{B}(\sigma) \equiv e^{-\tau\hat{H}_1/2} e^{\sqrt{\tau}\sigma \cdot \hat{\mathbf{v}}} e^{-\tau\hat{H}_1/2}, \quad (6)$$

with $\hat{\mathbf{v}} \equiv \{\sqrt{\lambda_1} \hat{v}_1, \sqrt{\lambda_2} \hat{v}_2, \dots\}$.

Monte Carlo methods can be used to evaluate the multi-dimensional integral of Eq. (5) efficiently. We follow the procedure [1, 17, 18] of turning the MC process

into an open-ended random walk (instead of Metropolis sampling of entire paths along imaginary time [12, 13]), because it facilitates the imposition of local constraints to deal with the sign/phase problem [18]. Each step in the random walk takes a Slater determinant $|\phi\rangle$ to a new determinant $|\phi'\rangle$:

$$|\phi'(\sigma)\rangle = \mathcal{B}(\sigma)|\phi\rangle, \quad (7)$$

where σ is sampled from $P(\sigma)$. Given sufficient propagation time one obtains a MC representation of the ground state: $|\Psi_G\rangle \doteq \sum_\phi |\phi\rangle$.

This straightforward approach, however, will generally lead to an exponential increase in the statistical fluctuations with the propagation time. One can easily understand the source of this by realizing that the one-body operators \hat{v} are generally complex, since λ_α usually cannot all be made positive in Eq. (4). As a result, the orbitals in $|\phi\rangle$ will become complex as the propagation proceeds. This is the phase problem referred to earlier. It is of the same origin as the sign problem that occurs when $\mathcal{B}(\sigma)$ is real. The phase problem is more severe, however, because for each $|\phi\rangle$, instead of a $+|\phi\rangle$ and $-|\phi\rangle$ symmetry [17], there is now an infinite set $\{e^{i\theta}|\phi\rangle\}$ ($\theta \in [0, 2\pi)$) from which the MC sampling cannot distinguish. At large propagation time, the phase of each $|\phi\rangle$ becomes random, and the MC representation of $|\Psi_G\rangle$ becomes dominated by noise.

In Ref. [1] the phaseless auxiliary field QMC method was presented to control the phase problem. The first ingredient of this method is an importance-sampling transformation using a *complex* importance function, $\langle\Psi_T|\phi\rangle$, where $|\Psi_T\rangle$ is a trial wave function. In the resulting random walk, a walker $|\phi\rangle$ is propagated to a new position $|\phi'\rangle$ in each step by

$$|\phi'(\sigma)\rangle = \mathcal{B}(\sigma - \bar{\sigma})|\phi\rangle. \quad (8)$$

As in Eq. (7), σ is sampled from $P(\sigma)$, but the propagator is modified to include a force bias, or shift [19]:

$$\bar{\sigma} = -\sqrt{\tau} \frac{\langle\Psi_T|\hat{v}|\phi\rangle}{\langle\Psi_T|\phi\rangle}. \quad (9)$$

A walker carries a weight w_ϕ which is updated according to

$$w_{\phi'} = W(\phi) w_\phi, \quad (10)$$

where $W(\phi)$ can be expressed in terms of the so-called local energy, E_L :

$$W(\phi) \doteq \exp \left[-\tau \frac{\langle\Psi_T|\hat{H}|\phi\rangle}{\langle\Psi_T|\phi\rangle} \right] \equiv \exp[-\tau E_L(\phi)]. \quad (11)$$

In the limit of an exact $|\Psi_T\rangle$, E_L is a real constant, the weight of each walker remains real, and the mixed

estimate for the energy is phaseless:

$$E_G = \frac{\langle\Psi_T|\hat{H}|\Psi_G\rangle}{\langle\Psi_T|\Psi_G\rangle} \doteq \frac{\sum_{\phi'} w_{\phi'} E_L(\phi')}{\sum_{\phi'} w_{\phi'}}. \quad (12)$$

With a general $|\Psi_T\rangle$ which is not exact, a natural approximation is to replace E_L in Eq.'s (11) and (12) by its real part, $\text{Re } E_L$, leading to a phaseless formalism for the random walk, with real and positive weights.

The second ingredient in the phaseless method involves a projection: the modified random walk is still “rotationally invariant” in the complex plane defined by $\langle\Psi_T|\phi\rangle$. With the propagation, the walkers will populate the complex plane symmetrically independent of their initial positions. In particular, a finite density of walkers will develop at the origin where the local energy $E_L(\phi)$ diverges, and this causes diverging fluctuations in the weights of walkers.

This problem, which is inherent of the “two-dimensional” nature of the random walk in the complex plane, can be controlled with an additional approximation, in which the random walk is projected to “one-dimension.” This is done, e.g., by multiplying the weight of each walker in each step by $\max\{0, \cos(\Delta\theta)\}$, where $\Delta\theta$ is the phase of $\langle\Psi_T|\phi'\rangle/\langle\Psi_T|\phi\rangle$. The projection ensures that the density of walkers vanish at the origin. Note that the projection has no effect when \hat{v} is real. This additional approximation and the importance-sampling procedures of Eq.'s (8) through (11) form the basis of the new phaseless AF QMC method.

III. IMPLEMENTATION WITH PLANEWAVES

The calculations reported in this paper were carried out in supercells using a planewave basis and periodic boundary conditions (PBC). Pseudopotentials are used as in DFT calculations to represent the electron-ion interaction, eliminating the core electrons from the Hamiltonian. The basis set consists of the M planewaves with kinetic energy $|\mathbf{k}|^2/2 < E_{\text{cut}}$, where the parameter E_{cut} is a cutoff energy.

In a planewave basis, the one-body operator \hat{H}_1 of Eq. (1) is the sum of the kinetic energy and the electron-ion interaction, and \hat{H}_2 represents the electron-electron interaction. These can be expressed as:

$$\begin{aligned} \hat{H}_1 &= -\frac{\hbar^2}{2m} \sum_{\mathbf{k},s} |\mathbf{k}|^2 c_{\mathbf{k},s}^\dagger c_{\mathbf{k},s} + \sum_{\mathbf{k},\mathbf{k}',s} V_L(\mathbf{k} - \mathbf{k}') c_{\mathbf{k},s}^\dagger c_{\mathbf{k}',s} \\ &+ \sum_{\mathbf{k},\mathbf{k}',s} V_{NL}(\mathbf{k}, \mathbf{k}') c_{\mathbf{k},s}^\dagger c_{\mathbf{k}',s} \\ \hat{H}_2 &= \frac{1}{2\Omega} \sum_{\mathbf{k},\mathbf{k}',s,s'} \sum_{\mathbf{q} \neq 0} \frac{4\pi e^2}{|\mathbf{q}|^2} c_{\mathbf{k}+\mathbf{q},s}^\dagger c_{\mathbf{k}'-\mathbf{q},s'}^\dagger c_{\mathbf{k}',s'} c_{\mathbf{k},s}. \end{aligned} \quad (13)$$

TABLE I: A summary of the binding energy BE (in eV), equilibrium bond length R_e (in a.u.) and harmonic vibrational frequency ω (in cm^{-1}) of the TiO molecule with two different pseudopotentials. The first, with $E_{\text{cut}} = 50 \text{ Ry}$ (50 Ry psp), was used in all ensuing DFT and QMC calculations. The second has a 64 Ry cut-off. The corresponding values of the cut-off radius, r_c , are listed in the footnotes (in units of a.u.). DFT results from both Perdew-Burke-Ernzerhof (PBE) GGA [27] and Perdew-Wang 92 LDA [28] functionals are shown, together with experimental values.

	BE	R_e	ω
Experiment[20, 21]	6.87 or 6.98	3.06	1009
50 Ry psp ^a	GGA	8.00	3.02 1005
	LDA	9.11	2.99 1040
64 Ry psp ^b	GGA	7.96	3.04 1008
	LDA	9.05	3.02 1044

^aO r_c : 1.45 (s), 1.55 (p); Ti r_c : 1.40 (s), 1.40 (p), 1.80 (d).
^bO r_c : 1.30 (s), 1.39 (p); Ti r_c : 1.35 (s), 1.35 (p), 1.52 (d).

Here $c_{\mathbf{k},s}^\dagger$ and $c_{\mathbf{k},s}$ are the creation and annihilation operators of an electron with momentum \mathbf{k} and spin s . $V_L(\mathbf{k} - \mathbf{k}')$ and $V_{NL}(\mathbf{k}, \mathbf{k}')$ are the local and non-local parts of the pseudopotential, respectively. Ω is the supercell volume, \mathbf{k} and \mathbf{k}' are planewaves within the cutoff radius, and the \mathbf{q} -vectors satisfy $|\mathbf{k} + \mathbf{q}|^2/2 < E_{\text{cut}}$.

A Hubbard-Stratonovich transformation is applied to decouple the electron-electron interaction \hat{H}_2 into a linear combination of one-body operators. The resulting one-body operators consist of density operators of the form $\hat{\rho}(\mathbf{q}) = \sum_{\mathbf{k},s} c_{\mathbf{k}+\mathbf{q},s}^\dagger c_{\mathbf{k},s}$. The number of auxiliary fields is proportional to the number of unique \mathbf{q} vectors that the basis allows, i.e., roughly eight times the number of planewaves in the basis.

Non-local pseudopotentials can be treated *exactly* within the present AF QMC formalism, and the use of separable forms leads to the same speed-up achieved in planewave DFT calculations [1]. This is to be compared with standard real-space DMC calculations where an additional locality approximation [22] is used for non-local pseudopotentials that depends on the overall quality of the trial wave function $|\Psi_T\rangle$. (In contrast, the fixed-node approximation in DMC only depends on the position of the nodal surface of $|\Psi_T\rangle$.) In order to minimize errors due to the locality approximation, small pseudopotential cut-off radii r_c tend to be used. This could result in harder pseudopotentials than otherwise required by transferability considerations. In the AF QMC, the use of non-local pseudopotentials with larger values r_c (determined only by transferability requirements) does not pose any additional difficulty.

TABLE II: A summary of the binding energy BE (in eV), equilibrium bond length R_e (in a.u.), and harmonic vibrational frequency ω (in cm^{-1}) of the MnO molecule with three different pseudopotentials. The first, with $E_{\text{cut}} = 64 \text{ Ry}$ and created from the design non-local (DNL) procedure, was used in all ensuing DFT and QMC calculations. Two other sets are also tested here, with 64 Ry and 82 Ry cut-off values and without DNL. The corresponding r_c values (in a.u.) are listed in the footnotes. Calculated results are from DFT GGA.

	BE	R_e	ω
Experiment [21]	3.70	3.11	832
64 Ry DNL psp ^a	5.11	3.11	822
64 Ry psp ^b	4.90	3.07	878
82 Ry psp ^c	4.99	3.09	845

^aO r_c : 1.45 (s), 1.55 (p); Mn r_c : 1.40 (s), 1.40 (p), 1.65 (d).

^bO r_c : 1.45 (s), 1.55 (p); Mn r_c : 1.40 (s), 1.40 (p), 1.65 (d).

^cO r_c : 1.05 (s), 1.02 (p); Mn r_c : 1.25 (s), 1.25 (p), 1.50 (d).

IV. RESULTS

In this paper, we apply the phaseless AF QMC method to calculate the binding energies of the transition metal oxide molecules TiO and MnO . Norm-conserving pseudopotentials are used, and the non-local part of the pseudopotential V_{NL} is represented using the separable Kleinman-Bylander (KB) form [23].

To obtain the trial wave function $|\Psi_T\rangle$ for each QMC calculation, a DFT calculation with the generalized gradient approximation (GGA) is carried out with the ABINIT [24] program, using the same pseudopotentials and planewave basis. $|\Psi_T\rangle$ is then taken as the single Slater determinant formed from the occupied single-particle orbitals obtained from this DFT calculation, with *no further optimization*. The random walkers are all initialized to $|\Psi_T\rangle$, so the many-body ground-state projection initiates from the GGA state. In addition, this $|\Psi_T\rangle$ is used in the QMC calculations to control the sign/phase problem as described in Section II.

The pseudopotentials were generated by the OPIUM program [25] using Ti^{++} , Mn^{++} , and neutral oxygen as reference configurations. The titanium and manganese semicore states ($3s^2 3p^6$) were included as valence states, so the Ti and Mn atoms contribute 12 and 15 valence electrons, respectively, while the O atom contributes 6 electrons.

Well-converged planewave cutoffs were 50 Ry for oxygen and titanium, and 64 Ry for manganese. These E_{cut} 's were chosen such that the resulting cut-off errors, systematically analyzed using DFT calculations, were much smaller than the expected QMC statistical errors. In addition, we have carried out QMC calculations on a $1 \times 1 \times 1$ TiO solid supercell with a 50 Ry and 60 Ry cutoff, respectively. The calculated energies are the same within statistical error bars ($\approx 0.1 \text{ eV}$), confirming basis conver-

TABLE III: A comparison between LAPW and pseudopotential calculations for non spin-polarized TiO in a $7 \times 7 \times 14$ a.u.³ supercell. We show the equilibrium bond length R_e (in a.u.) and harmonic vibrational frequency ω (in cm⁻¹) from DFT, using both GGA and LDA. The two OPIUM pseudopotentials are the same as those in Table I.

		R_e	ω
LAPW	GGA	3.01	1057
	LDA	2.97	1097
50 Ry psp	GGA	2.96	1060
	LDA	2.94	1095
64 Ry psp	GGA	2.99	1058
	LDA	2.97	1091

gence at the correlated level. The Mn pseudopotential is created using the design non-local pseudopotential procedure [26]. This enhances the pseudopotential transferability by exploiting the flexibility contained in the separable KB form of the nonlocal pseudopotential.

The accuracy of the pseudopotentials was examined with DFT calculations of binding energies, as well as the equilibrium bond length and harmonic vibrational frequencies. In Tables I and II, we summarize our calculations of these properties for different OPIUM pseudopotentials. In both cases, increasing the hardness of our pseudopotentials did not lead to significant changes in the calculated properties. We have also done some of these calculations using Troullier-Martins [29] pseudopotentials with the same cutoff radii, and little difference was found. Moreover, our LDA results for the bondlengths for TiO and MnO, $R_e = 2.99$ a.u. and 3.05 a.u., are in reasonable agreement with the all-electron LDA values ($R_e = 3.020$ a.u. and 3.032 a.u.) [30] and those obtained with the Hartwigsen-Goedecker-Hutter pseudopotentials [30]. The TiO results of R_e and ω also compare favorably with the calculations of Ref. [31].

As a further check on the pseudopotentials, we have carried out a comparison between pseudopotential and all-electron LAPW calculations. The latter is computationally more costly, so we limited the comparison to a $7 \times 7 \times 14$ a.u.³ supercell for non spin-polarized TiO molecule. Our results for the calculated equilibrium bond length and angular frequency of vibration are summarized in Table III. The close agreement between the LAPW and the pseudopotential results gives further evidence on the reliability of the pseudopotentials.

Clearly these tests on the quality of the pseudopotentials are far from perfect. Our pseudopotentials are all DFT-based, and the tests are with DFT calculations. For *sp*-bonded systems, we have done plane-wave Hartree-Fock (HF) calculations using OPIUM DFT pseudopotentials, and compared with all-electron HF results. In general, these tend to be quite consistent with the DFT tests, and often good agreement at the HF level is found

TABLE IV: A summary of the calculated binding energy of the molecule TiO for different supercells. Supercell dimensions are given in a.u. and binding energies are in eV. The QMC statistical errors are in the last two digits, and are indicated in parentheses. At the DFT GGA level, the binding energy converges to 8.00 eV.

	GGA	QMC
$10 \times 11 \times 17$	7.46	6.59(20)
$12 \times 12 \times 15$	7.77	6.98(21)
$14 \times 14 \times 15$	7.94	7.08(21)
∞	8.00	

TABLE V: The calculated total ground-state energy of Mn for different supercells. Supercell dimensions are in a.u. and energies are in eV. The QMC statistical errors are in the last digit, and are shown in parentheses.

	GGA	QMC
$11 \times 12 \times 15$	-2766.66	-2766.40(5)
$12.55 \times 13.69 \times 17.11$	-2766.38	-2765.66(4)
$14 \times 14 \times 15$	-2766.32	-2765.89(9)
$15.4 \times 15.4 \times 16.5$	-2766.25	-2765.74(8)
∞	-2766.20	

when good test results have been obtained from DFT calculations. Of course, the suitability of a DFT or HF pseudopotential (i.e., derived from independent-particle procedures) for many-body calculations is a separate issue, which our tests do not address. Empirically, such pseudopotentials have been widely used in many-body calculations and have been quite successful.

The use of PBC with a planewave basis requires supercells that are large enough to control spurious interactions between the periodic images of the system under study. We studied convergence with respect to such size effects using both ABINIT and QMC calculations. Representative results are shown in Tables IV and V.

Estimating the size-effects in the AF QMC calculations is complicated by the presence of finite Trotter time-step (τ) errors. The QMC values shown in Tables IV and V are final values after extrapolations in τ , as discussed further below. The range of supercells shown in Table IV corresponds to about 12,000-17,000 planewaves in our basis. For the Ti atom, the largest two supercells resulted in a degeneracy of the highest-lying occupied *d*-orbitals in the density functional calculations. To break the degeneracy, these supercells were modified to $11.6 \times 12 \times 15$ a.u.³ and $13.5 \times 14 \times 15$ a.u.³, respectively. The fully converged value of the DFT GGA TiO binding energy is 8.00 eV, as shown. For the AF QMC calculations, the binding energies for the larger sizes are converged to well within the statistical errors.

Table V shows the energy of the Mn atom for different supercell sizes. The corresponding number of planewaves

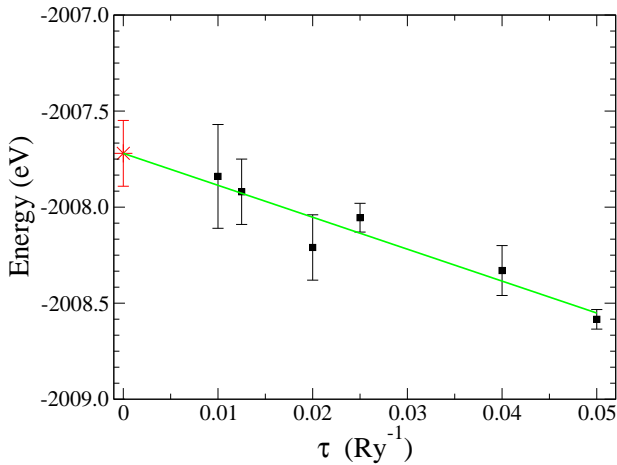


FIG. 1: QMC time-step τ dependence of the total energy of the TiO molecule. A $10 \times 11 \times 17$ a.u.³ supercell was used. The solid line is a linear fit to the calculated QMC energies (solid squares). The final extrapolated energy $E = -2007.72(17)$ eV is shown as a star.

is between 17,000 and 34,000. As can be seen, the QMC energy is converged to less than the statistical error for the $14 \times 14 \times 15$ supercell, although for the smaller supercells, the finite-size errors are significant both in GGA and QMC. The MnO molecule, on the other hand, exhibits a much smaller size effect, with QMC energies of $-3195.50(11)$ eV and $-3195.58(7)$ eV for the $11 \times 12 \times 15$ and $14 \times 14 \times 15$ supercells, respectively.

The QMC Trotter errors were examined by studying the individual time-step dependence for the atoms and the molecule using a particular supercell size. Figure 1, for example, shows the Trotter extrapolation for the TiO molecule, done with a $10 \times 11 \times 17$ supercell. The Trotter behavior obtained from this procedure was then used to extrapolate the QMC data of other supercell sizes, for which calculations were performed with the time step fixed at $\tau = 0.025$ Ry⁻¹. The final extrapolated results are what is shown (e.g., in Table IV). Figure 2 shows the time-step dependence of MnO, which exhibits a quadratic behavior compared to the more linear dependence in Fig. 1 for TiO. The Mn and O atoms exhibit much smaller finite- τ errors, as is also the case with the Ti atom (not shown).

Table VI summarizes the results for the molecular binding energies. For comparison we also include results from a recent diffusion Monte Carlo study by Wagner and Mitas [4]. As mentioned, our AF QMC calculations use a single-determinant trial wave functions obtained from a DFT GGA calculation, without a Jastrow factor or any further optimization to the determinant. We see that the calculated binding energies from AF QMC and those from DMC [4] with trial wave functions containing

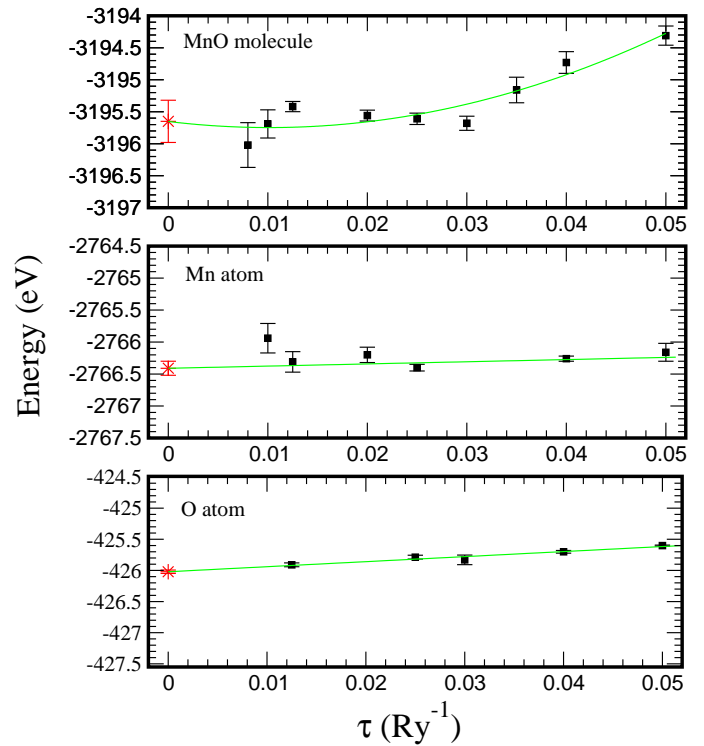


FIG. 2: QMC time-step τ dependence of MnO, Mn, and O. An $11 \times 12 \times 15$ a.u.³ supercell was used for MnO and Mn, and a $10 \times 11 \times 17$ a.u.³ supercell for oxygen. The solid line is a least-squares fit to the QMC energies (solid squares). The final extrapolated values are shown as a star. MC statistical error bars are indicated.

either an optimized hybrid B3LYP determinant or multiple determinants from MCSCF are in good agreement with each other and with experiment. DMC with a trial wave function containing the Jastrow and a single Slater determinant from HF, on the other hand, gives somewhat worse agreement with experiment. We have not carried out AF QMC calculations using an HF trial wave function for these molecules. In several *sp*-bonded molecules, DFT and HF-generated trial wave functions showed little difference in the calculated energies in AF QMC.

We have also included in Table VI the results for the binding energy of the O₂ molecule. Because of the short bond length of this molecule ($R_e = 2.281$ a.u.), a harder pseudopotential was used, with a higher E_{cut} of 82 Ry and smaller values for r_c (last entry in Table II). At the DFT GGA level the binding energy is 5.72 eV. Our QMC results shown in Table VI were obtained using a supercell of size $8 \times 9 \times 11$ a.u.³. Additional QMC and DFT calculations with a larger supercell of $11 \times 12 \times 13$ a.u.³ have verified that the finite-size effects are within our statistical error bars (≈ 0.1 eV). Again, we see that the agreement with experiment is very good.

TABLE VI: A summary of the binding energies of the molecules TiO, MnO, and O₂. Calculated results from the present QMC method and diffusion Monte Carlo (TiO and MnO from Ref. [4], and O₂ from Ref. [32]) are shown, together with experimental values (TiO from Refs. [20, 21], MnO from Ref. [20], and O₂ from Ref. [32]). Equilibrium experimental bond lengths were used in the molecule calculations. Our QMC used as trial wave function a single Slater determinant from DFT GGA. The trial wave functions used in DMC are indicated in the footnotes. All energies are in eV, and the experimental zero point energy is added to each molecule.

	TiO	MnO	O ₂
Experiment	6.98	3.70	5.1152(9)
	6.87		
DMC (HF) ^a	6.3(1)	2.9(1)	4.84(2)
DMC (B3LYP) ^b	6.9(1)	3.4(2)	
DMC (MCSCF) ^c	6.7(2)	3.4(2)	
Present QMC	7.02(21)	3.79(34)	5.12(10)

^aTrial w.f. is a (HF 1-determinant)×Jastrow.

^bTrial w.f. is a (DFT B3LYP 1-determinant)×Jastrow.

^cTrial w.f. is a (MCSCF multi-determinant)×Jastrow.

Finally, we comment briefly on the computational cost. As mentioned, the use of planewaves for isolated molecules is somewhat disadvantageous even at the density-functional level, because of the need for large supercell sizes to reduce the spurious interactions between the images of the molecule. The number of planewaves, M , is proportional to the supercell volume, and the computational cost scales with M as $M \ln M$. (In addition, it scales quadratically with the number of electrons.) As a result, these planewave AF QMC calculations are com-

putationally rather demanding, especially with transition metal oxides. For instance, the ground-state energy of the MnO molecule in Fig. 2 at the single Trotter step of $\tau = 0.008 \text{ Ry}^{-1}$ (with an error bar of 0.35 eV) was obtained from running on an Intel XEON cluster (3.2 GHz) for about 150 hours using 72 processors.

In summary, we have presented the first study of transition metal oxide molecules by AF QMC. We have shown that the binding energies of TiO and MnO calculated with the new phaseless AF QMC method [1] are in good agreement with experiment, and are comparable to the best results obtained from diffusion Monte Carlo [4]. It is encouraging that a trial wave function of only DFT single Slater determinants was sufficient for the phaseless QMC method to reach this accuracy. Together with previous results for *sp*-bonded systems [1, 15], the present study indicates that the phaseless method is a robust QMC method. Complementary to standard DMC, it offers a promising approach for the computation of correlation effects in real materials.

V. ACKNOWLEDGMENTS

We would like to thank E. J. Walter for many useful discussions, and for carrying out the LAPW calculations. This work was supported by ONR Grants N000149710049 and N000140110365, NSF, and DOE’s Computational Materials Science Network. Computations were carried out in part at the Center for Piezoelectrics by Design (CPD), the SciClone Cluster at the College of William and Mary, the National Center for Supercomputing Applications (NCSA), and the San Diego Supercomputer Center (SDSC) center.

[1] S. Zhang and H. Krakauer, Phys. Rev. Lett. **90**, 136401 (2003).
[2] W. M. C. Foulkes, L. Mitas, R. J. Needs, and G. Rajagopal, Rev. Mod. Phys. **71**, 33 (2001).
[3] Svetlana Sokolova and Arne Lüchow, Chem. Phys. Lett. **320**, 421 (2000).
[4] Lucas Wagner and Lubos Mitas, Chem. Phys. Lett. **370**, 412 (2003).
[5] Ji-Woo Lee, Lubos Mitas, and Lucas Wagner, cond-mat/0411247 (2004).
[6] R. J. Needs and M. D. Towler, Int. J. Mod. Phys. B, **17**, 5425 (2003).
[7] W. Kohn, Rev. Mod. Phys. **71**, 1253 (1999).
[8] K. E. Schmidt and M. H. Kalos, in *Applications of the Monte Carlo Method in Statistical Physics*, ed. by K. Binder (Springer Verlag, Heidelberg, 1984).
[9] E. Y. Loh Jr., J. E. Gubernatis, R. T. Scalettar, S. R. White, D. J. Scalapino, and R. L. Sugar, Phys. Rev. B **41**, 9301 (1990).
[10] D. M. Ceperley and B. J. Alder, Phys. Rev. Lett. **45**, 566 (1980).
[11] W. Kohn, Rev. Mod. Phys. **71**, 1253 (1999).
[12] R. Blankenbecler, D. J. Scalapino, and R. L. Sugar, Phys. Rev. D **24**, 2278 (1981).
[13] G. Sugiyama and S. E. Koonin, Ann. Phys. (NY) **168**, 1 (1986).
[14] J. Carlson, J. E. Gubernatis, G. Ortiz, and Shiwei Zhang, Phys. Rev. B **59**, 12788 (1999).
[15] Shiwei Zhang, Henry Krakauer, Wissam Al-Saidi, and Malliga Suewattana, Comp. Phys. Comm. **169**, 394 (2005).
[16] R. L. Stratonovich, Sov. Phys. Dokl. **2**, 416 (1958); J. Hubbard, Phys. Rev. Lett. **3**, 77 (1959).
[17] Shiwei Zhang, J. Carlson, and J. E. Gubernatis, Phys. Rev. B **55**, 7464 (1997).
[18] Shiwei Zhang, in *Theoretical Methods for Strongly Correlated Electrons*, ed. by D. Senechal, A.-M. Tremblay, and C. Bourbonnais (Springer 2003).
[19] Naomi Rom, D. M. Charutz, and Daniel Neuhauser, Chem. Phys. Lett. **270**, 382 (1997).

- [20] K. P. Huber and G. Herzberg, Molecular Spectra and Molecular Structures. IV. Constants of Diatomic Molecules, Van Nostrand, New York, 1979.
- [21] H. P. Loock, B. Simard, S. Wallin, and C. Linton, *J. Chem. Phys.* **109**, 8980 (1998).
- [22] L. Mitas, Eric L. Shirley, and David M. Ceperley, *J. Chem. Phys.* **95**, 3467 (1991).
- [23] L. Kleinman and D. M. Bylander, *Phys. Rev. Lett.* **48**, 1425 (1982).
- [24] X. Gonze, J. -M. Beuken, R. Cara- cas, F. Detraux, M. Fuchs, G. -M. Rignanese, L. Sindic, M. Verstraete, G. Zerah, F. Jollet, M. Torrent, A. Roy, M. Mikami, Ph. Ghosez, J. -Y. Raty, and D. C. Allan, *Comp. Mat. Sci.* **25**, 478 (2002).
- [25] Andrew M. Rappe, Karin M. Rabe, Efthimios Kaxiras, and J. D. Joannopoulos, *Phys. Rev. B* **41**, R1227 (1990).
- [26] Nicholas J. Ramer and Andrew M. Rappe, *Phys. Rev. B* **59**, 12471 (1999).
- [27] J. P. Perdew, K. Burke, and M. Ernzerhof, *Phys. Rev. Lett.* **77**, 3865 (1996).
- [28] J. P. Perdew and Y. Wang, *Phys. Rev. B* **45**, 13244 (1992).
- [29] N. Troullier and J. L. Martins, *Phys. Rev. B* **43**, 1993 (1991).
- [30] C. Hartwigsen, S. Goedecker, and J. Hutter, *Phys. Rev. B* **58**, 3641 (1998).
- [31] T. Albaret, F. Finocchi, and C. Noguera, *Faraday Discuss.* **106**, 155 (1997)
- [32] Jeffery C. Grossman, *J. Chem. Phys.* **117**, 1434 (2002).